Relativistic-induced opacity of electron-positron plasmas

Jian Huang[1,2], S. M. Weng[1,2,†], X. L. Zhu[1,2], X. F. Li[1,2], M. Chen[1,2], M. Murakami[3], Z. M. Sheng[1,2,4,5,‡]

[1] Key Laboratory for Laser Plasmas (MoE), School of Physics and Astronomy, Shanghai Jiao Tong University, Shanghai 200240, China

[2] Collaborative Innovation Center of IFSA, Shanghai Jiao Tong University, Shanghai 200240, China

[3] Institute of Laser Engineering, Osaka University, Osaka 565-0871, Japan

[4] SUPA, Department of Physics, University of Strathclyde, Glasgow G4 0NG, UK

[5] Tsung-Dao Lee Institute, Shanghai Jiao Tong University, Shanghai 200240, China

E-mail: [†]wengsuming@gmail.com, or [‡]z.sheng@strath.ac.uk

Abstract. The interaction of intense electromagnetic waves with electron-positron (e^-e^+) plasmas is studied by particle-in-cell simulations and theoretical analysis. It is found that an initial underdense e^-e^+ plasma can become opaque under the irradiation of a relativistically intense laser pulse. The strong ponderomotive force of the relativistic laser pulse and the small mass density of the e^-e^+ plasma can combine to induce the efficient pile-up of the electrons and positrons at the front of the laser pulse. Therefore, the local plasma density at the laser pulse front increases dramatically and finally the initial underdense e^-e^+ plasma becomes opaque. This relativistic-induced opacity effect of e^-e^+ plasmas is opposite to the well-known relativistic-induced transparency effect, in which an initial overdense electron-ion plasma can become transparent to a relativistically intense laser pulse. Further, the significant red shift of reflected lights as well as the efficient generation of energetic positrons are investigated in the relativistic-induced opacity of e^-e^+ plasmas. This relativistic-induced opacity effect is a peculiar phenomenon in the e^-e^+ plasmas, which may be encountered in the high-energy astrophysical phenomena or in the interactions of intense lasers with matters in the laboratories.

Submitted to: *Plasma Phys. Control. Fusion*

Contents

1. Introduction

Electron-positron (e^-e^+) plasmas exist widely in the universe [1], they are intensively studied in the research of black holes [2], pulsar wind nebulaes [3], relativistic jets [4] and quasars [5]. Moreover, the study of e^-e^+ plasmas plays an important role in understanding the properties and origins of gamma-rays bursts, and may provide necessary information about the evolution of very early universe [6, 7]. The rapid development of laser technology in the last decades [8] provides a unique approach to creating extreme astrophysical-like conditions, and thus the study of astronomical phenomena in the laboratory becomes possible [9, 10]. In particular, many mechanisms are suggested for the production of e^-e^+ pair plasmas by intense lasers [11, 12]. If the electric field is sufficiently strong, i.e. beyond the Schwinger critical field $\sim 10^{16}$ V/cm, the virtual e^-e^+ pairs in the vacuum can be transformed into real e^-e^+ pairs [13]. To produce e^-e^+ pairs via this Schwinger effect, however, the required extremely high laser intensity ($\sim 10^{29}$ W/cm^{-2}) is far beyond the currently available laser intensity ($\sim 10^{22}$ W/cm^{-2}). At present, the Bethe-Heiter process is still the dominant mechanism in experiments for the production of e^-e^+ plasmas [14, 15], where the positron density of $\sim 10^{16}$ cm^{-3} has been achieved via this mechanism [16, 17, 18]. Further, the multi-photon Breit-Wheeler process could dominate the production of e^-e^+ plasmas when the laser intensity is greater than 10^{22} W/cm^2 [19, 20]. Then dense e^-e^+ plasmas could be generated in the interactions of such ultra-intense laser pulses with near-critical-density plasmas [21, 22], solid targets [23, 24, 25], or energetic electron beams [26, 27]. The numerical simulations show that the high-yield (1.05×10^{11}) and over-dense (4×10^{22} cm^{-3}) GeV positron beams may be produced by using 10 PW-class lasers [21, 25].

As a typical kind of equal-mass plasmas, e^-e^+ plasmas have some peculiar features that are distinct from those of usual electron-ion plasmas. Above all, the contribution of positrons to the e^-e^+ plasma frequency is identical to that of electrons. Therefore, a non-relativistic electromagnetic wave can propagate into an e^-e^+ plasma when its electron density $n_e < 0.5n_c$, i.e. the critical density for the e^-e^+ plasmas is only half of that for the electron-ion plasmas [28, 29]. Further, the electrons and positrons have the same cyclotron frequency and the opposite direction of gyration in an external magnetic field. This special symmetry causes that some well-known phenomena in the electron-ion plasmas, such as Faraday effect, disappear in the e^-e^+ plasmas [28, 29, 30]. In addition, it is found that stimulated Brillouin backscattering is strongly enhanced in e^-e^+ plasmas, in contrast to the suppression of stimulated Raman scattering [31].

In this paper, we report a peculiar phenomenon in e^-e^+ plasmas that relativistic-induced opacity may occur when an intense electromagnetic wave propagates in an underdense e^-e^+ plasma, in contrast to the relativistic-induced transparency of an overdense electron-ion plasma. As it is well known, an electromagnetic wave with a frequency ω cannot propagate into an electron-ion plasma whose electron number density is higher than the so-called critical density $n_c = m_e\epsilon_0\omega^2/e^2$. With a sufficiently intense laser pulse, however, the electron oscillation motion in the laser electromagnetic field may become relativistic and thus the effective electron mass increases by a Lorentz factor γ_e. As a result, a relativistically intense laser pulse may penetrate into a classically overdense electron-ion plasma, i.e. relativistic-induced transparency takes place [32, 33, 34, 35, 36, 37, 38]. In contrast, here we find that the electrons and positrons in e^-e^+ plasmas tend to be pushed forward by the radiation pressure of relativistic laser pulses rather than to oscillate transversally in the laser field. Consequently, the electrons and positrons will pile-up and form a high density peak at the front of the laser pulse, which can finally prevent the laser pulse from propagating into an underdense e^-e^+ plasma. The similar density pile-up under the irradiation of a relativistic laser pulse has been studied previously in electron-ion plasmas[39, 40]. Such a relativistic-induced opacity is a fundamental feature of e^-e^+ plasmas, which is not only interesting for the study of laser-produced e^-e^+ plasmas in laboratories but also astronomical phenomena associated with e^-e^+ plasmas.

2. Numerical Simulations and Analysis

We find this relativistic-induced opacity effect of underdense e^-e^+ plasmas by accident in the 1D-3V particle-in-cell (PIC) simulations using the Osiris code [41]. In each simulation, an intense laser pulse with a wavelength $\lambda = 1$ μm is incident along the x-axis into a semi-infinite e^-e^+ plasma at $x \geq 5\lambda$. The simulation box has a length of 100λ with a spatial resolution $\Delta x = \lambda/100$, and each particle species is represented by 1000 macroparticles per cell. The quadratic interpolation and the SIMD (single instruction, multiple data) accelerated pusher are used for the macroparticles. The standard Yee solver is used for the Maxwell equations, and no smoothing is applied

to the electromagnetic fields or the currents. To minimize the numerical dispersion relation, the normalized time step is set to be slightly smaller than the spatial cell size, and the corresponding CFL value is 0.999. The laser pulse is either linearly or circularly polarized, and its intensity remains constant after a rising edge of five wave cycles. The density of e^-e^+ plasma increases from zero to a constant value in the region $5\lambda \leq x \leq 15\lambda$, and then remains constant in the region $x \geq 15\lambda$. The initial temperatures of the electrons and positrons are both 1 keV. We have also performed many test simulations with different laser rising edges, plasma temperatures and density rising ramps, and have found that the relativistic-induced opacity effect is not sensitive to the length of the laser rising edge, or the plasma temperature and density rising ramp length.

In all simulations, the electron and positron number densities are both lower than 5.5×10^{20} cm^{-3}. At such low densities, the electron-positron annihilation effect [30, 42, 43] can be ignored within the simulation time ($<$ 500 fs). For convenience, normalized variables will be used below. The time, length, electric and magnetic field are normalized to $2\pi/\omega$, λ, $m_e\omega c/e$ and $m_e\omega/e$, respectively. In particular, we introduce the dimensionless amplitude of laser electric field $a \equiv eE/m_e\omega c$, which is related to laser intensity I by $a^2 = I\lambda^2/1.37 \times 10^{18}\mathrm{Wcm}^{-2}\mu\mathrm{m}^2$ for linear polarization, or $a^2 = I\lambda^2/2.74 \times 10^{18}\mathrm{Wcm}^{-2}\mu\mathrm{m}^2$ for circular polarization. The laser pulse is non-relativistic when a is much smaller than one. Conversely, the pulse is relativistic when a is comparable to or larger than one.

2.1. Qualitative Description

The interactions of a non-relativistic or relativistic laser pulse with a same underdense e^-e^+ plasma ($n_e = 0.1n_c$) are displayed in Fig. 1 and Fig. 2, respectively. For the non-relativistic laser pulse ($a = 0.05 \ll 1$), we find that it can easily propagate into the underdense e^-e^+ plasma with $n_e = 0.1n_c$ for either the linear polarization [Fig. 1(a)] or circular polarization [Fig. 1(b)] case. In these non-relativistic cases, the perturbations on the electron and positron densities during the laser propagation are relatively small, and there is nearly no particles piled-up at the front of the laser pulses.

On the contrary, the relativistic laser pulse ($a = 1$) cannot propagate into the underdense e^-e^+ plasma with $n_e = 0.1n_c$. Except for the first few wave cycles of the rising edge, the main part of the relativistic laser pulse is prevented from penetrating into the e^-e^+ plasma as shown in Fig. 2. This illustrates a peculiar phenomenon of e^-e^+ plasmas that an underdense e^-e^+ plasma can become opaque under the irradiation of a relativistic laser pulse. This phenomenon stands in stark contrast to the relativistic-induced transparency of electron-ion plasmas, in which an overdense electron-ion plasma can become transparent with a relativistic laser pulse [32, 33, 34, 35, 36, 37, 38].

To better understand the distinct phenomena displayed in Fig. 1 and Fig. 2, the time evolutions of the momenta of some representative particles under the irradiations of the non-relativistic and relativistic laser pulses are compared. Under the irradiation

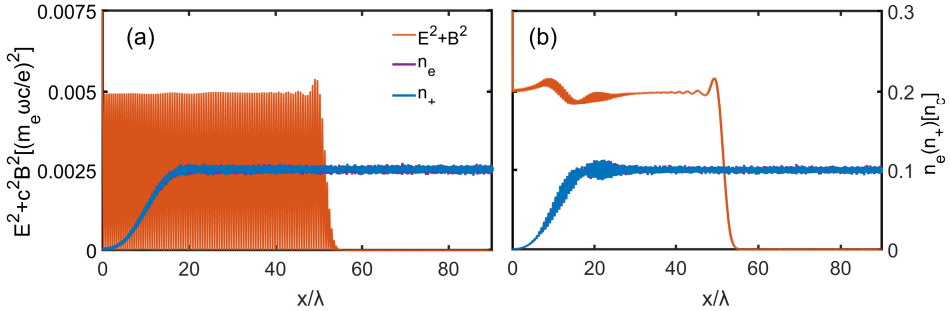

Figure 1. (Color online) The propagation of a non-relativistic laser pulse into an underdense e^-e^+ plasma. The laser field energy density $E^2 + B^2$ (red curve), electron density n_e (green curve), and positron density n_+ (blue curve) obtained in the PIC simulation of the laser interaction with the e^-e^+ plasma at $t = 60\lambda/c$. The initial electron and positron densities are $n_e = n_+ = 0.1n_c$. The laser has a non-relativistic amplitude $a = 0.05$, and it is (a) linearly or (b) circularly polarized.

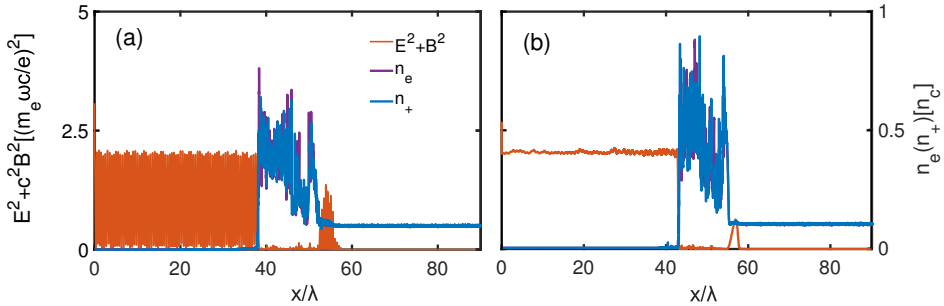

Figure 2. The opacity of an underdense e^-e^+ plasma in the irradiation of a relativistic laser pulse. Except $a = 1$, all other parameters are the same as those in Fig. 1.

of a non-relativistic laser pulse ($a = 0.05$), the electrons as well as the positrons of an underdense e^-e^+ plasma are mainly oscillating in the transverse direction as shown in Fig. 3(b). And their longitudinal velocities in Fig. 3(a) are obviously lower than the propagation velocity of the laser pulse that is close to the speed of light in a vacuum. Therefore, no particles can be trapped and accumulated ahead of the laser pulse front, and hence this non-relativistic laser pulse can propagate easily in the underdense e^-e^+ plasma. Under the irradiation of a relativistic laser pulse ($a = 1$), however, the electrons and positrons will be efficiently pushed forward in the longitudinal direction by the laser ponderomotive force. In this case, the longitudinal motions of the particles overwhelms their transverse oscillations as shown in Figs. 4(a) and 4(b). More importantly, Fig. 4(a) illustrates that the longitudinal velocities of the electrons become relativistic and comparable to the speed of light in a vacuum. Therefore, the electrons as well as the positrons will pile-up ahead of the laser pulse front. As a result, a high density peak is formed at the laser-plasma interface, which finally prevents the relativistic laser pulse from propagating into the underdense e^-e^+ plasma as shown in Fig. 2.

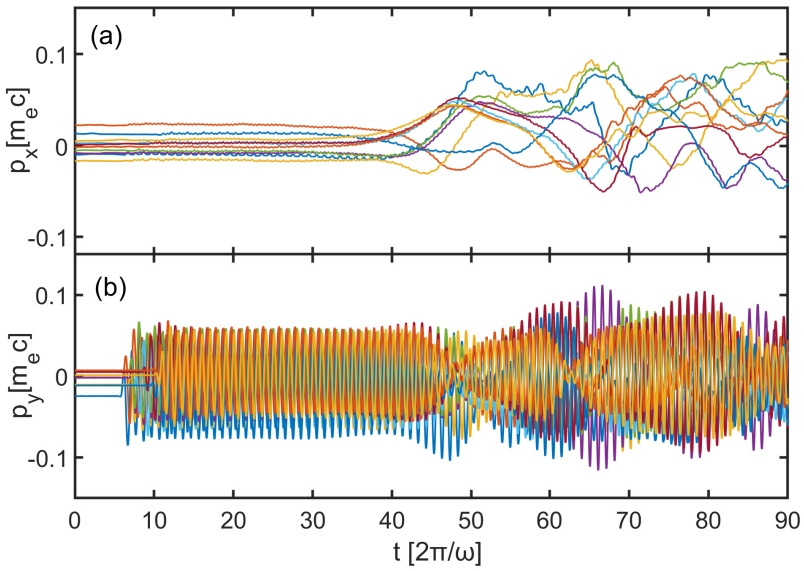

Figure 3. Time evolutions of the longitudinal (p_x) and transverse (p_y) momenta of some representative electrons and positrons under the irradiation of a non-relativistic laser pulse, obtained in the PIC simulation corresponding to Fig. 1(a).

2.2. Quantitative Analysis

To quantitatively analyse the interaction of laser pulses with e^-e^+ plasmas, the dependence of the laser front forward velocity on the laser amplitude is investigated.

In the transparency case with a non-relativistic laser pulse, the forward velocity of the laser front is approximate to the laser group velocity

$$v_g = \frac{\partial \omega}{\partial k} = c\sqrt{1 - \frac{2n_e}{n_c}}, \tag{1}$$

in which the dispersion relation $\omega^2 = 2\omega_p^2 + c^2k^2$ in e^-e^+ plasmas is employed with $\omega_p = \sqrt{n_e e^2/\epsilon_0 m}$. The above equation indicates that the forward velocity of the laser front is independent of the laser intensity in the transparency cases.

In the relativistic-induced opacity of an underdense e^-e^+ plasma, however, a dense e^-e^+ layer will be formed ahead of the laser pulse. Driven by the laser ponderomotive force, this dense e^-e^+ layer will move forward quickly. Assuming the interface between the laser pulse and the e^-e^+ plasma moves at a steady speed v_b, the momentum flux balance in the boosted frame moving with the interface can be obtained by using a quasi-stationary laser piston model as

$$\frac{2I}{c}\frac{1-\beta_b}{1+\beta_b} = 4\gamma_b^2 m_e n_e v_b^2, \tag{2}$$

where $\beta_b = v_b/c$ and $\gamma_b = (1-\beta_b^2)^{-1/2}$. Except for the replace of $m_i n_i$ by $2m_e n_e$, the above equation is analogous to the momentum flux conservation equation in the hole-boring radiation pressure acceleration of electron-ion plasmas by intense laser pulses

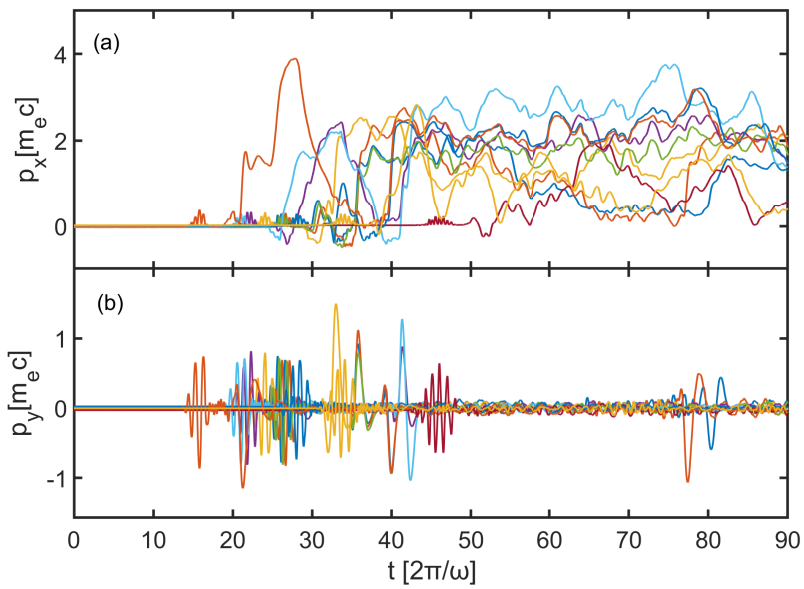

Figure 4. Time evolution of the longitudinal (p_x) and transverse (p_y) momenta of some representative electrons and positrons under the irradiation of a relativistic laser pulse, obtained in the PIC simulation corresponding to Fig. 2(a).

[44, 45]. From Eq. (2), the forward velocity of the interface between the laser pulse and the e^-e^+ plasma can be solved as

$$\frac{v_b}{c} = \beta_b = \frac{\sqrt{H}}{1+\sqrt{H}}, \tag{3}$$

with $H = I/2m_en_ec^3$. For circular polarization it holds $H = a^2n_c/2n_e$, and for linear polarization $H = a^2n_c/4n_e$. Correspondingly, the mean energies of the accelerated positrons (ε_+) and the electrons (ε_e) are about

$$\frac{\varepsilon_+}{m_ec^2} = \frac{\varepsilon_e}{m_ec^2} = \frac{2H}{1+2\sqrt{H}}. \tag{4}$$

As shown in Fig.5, there is an obvious fall in the forward velocity of the laser front when the laser amplitude increases from $a = 0.3$ to $a = 0.4$ for a given underdense e^-e^+ plasma with $n_e = n_+ = 0.1n_c$. This implies that the initial underdense e^-e^+ plasma becomes opaque when the laser amplitude is larger than the threshold value for the relativistic-induced opacity ($a_{th} \sim 0.4$). The e^-e^+ plasma should be transparent in the $a < a_{th}$ region, where the forward velocity of the laser front is independent of the laser intensity. Indeed, the forward velocity of the laser front obtained from the PIC simulations is always about $0.9c$ for $a \leq 0.3$, which is approximate to the laser group velocity ($v_g \simeq 0.894c$) estimated by Eq. (1) with $n_e = 0.1n_c$. On the contrary, the forward velocity of the laser front increases with the increasing laser amplitude in the relativistic-induced opacity region with $a \geq a_{th}$. As displayed in Fig.5, the PIC simulation results agree well with the theoretical predictions from Eq. (3) for both circular and linear polarization for $a \geq 0.4$. In particular, the forward velocity of the laser front becomes comparable to the speed of light in a vacuum when $a \geq 1$. This

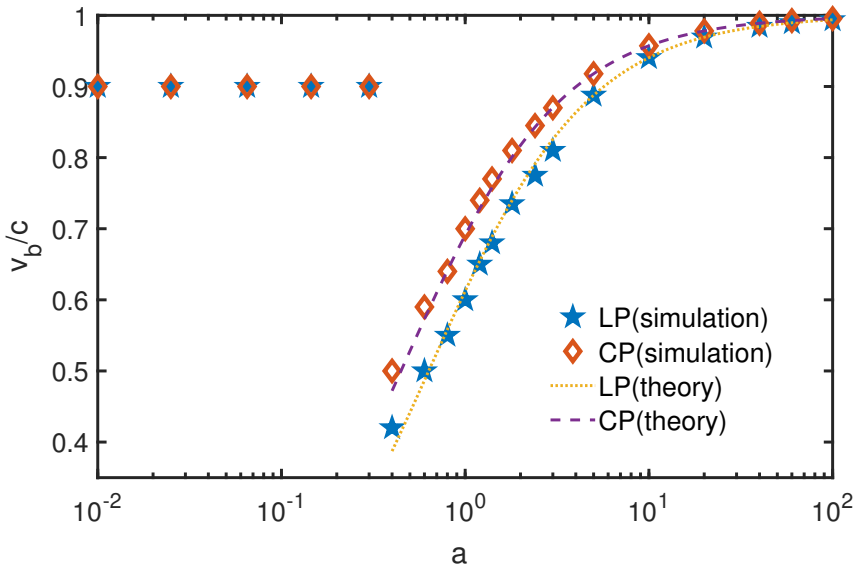

Figure 5. The forward velocity of the laser front as a function of the laser amplitude a when an intense laser pulse irradiates onto an underdense e^-e^+ plasma with $n_e = n_+ = 0.1n_c$. Here, the laser front is defined as the place where the local laser intensity is equal to the half of the incident laser intensity in a vacuum. The theoretical estimated values by Eq. (3) are compared with the PIC simulation results for both the linear polarization (LP) and circular polarization (CP) cases.

means that the interface between the relativistic laser pulse and the underdense e^-e^+ plasma usually moves forward at a relativistic speed in the relativistic-induced opacity scenario.

To estimate the threshold laser amplitude (a_{th}) for the relativistic-induced opacity, we assume that the plasma density of the pile-up layer is uniform. The initial underdense plasma density is assumed to be n_e, the normalized forward velocity of the laser front is $\beta_b = v_b/c$, the normalized velocity of the accelerated particles is $\beta_p = v_p/c$. According to the conservation of particle number, the plasma density of the pile-up layer (in the laboratory frame) will increase to $n_e\beta_p/(\beta_p - \beta_b)$ due to the density pile-up. Because of the Lorentz contraction of the longitudinal plasma length, the plasma density of the pile-up layer will be further increased by a Lorentz factor $\gamma_b = (1 - \beta_b^2)^{-1/2}$ in the co-moving frame with the laser-plasma interface. Therefore, the plasma density of the pile-up layer should be modified as $n_e^{'} = n_e\gamma_b\beta_p/(\beta_p - \beta_b)$ in the co-moving frame with the laser-plasma interface. To realize the relativistic-induced opacity effect, $n_e^{'}$ should be larger than $0.5n_c$, here $0.5n_c$ is the critical density of the e^-e^+ plasma for non-relativistic laser pulses. Therefore, threshold laser amplitude a_{th} can be estimated from the equality:

$$n_e^{'} = \frac{n_e\gamma_b\beta_p}{\beta_p - \beta_b} = 0.5n_c \tag{5}$$

where β_b and β_p are given by Eq. (3) and Eq. (4), respectively. Combining Eqs. (3), (4) and (5), the following implicit expression can be derived for the estimation of the

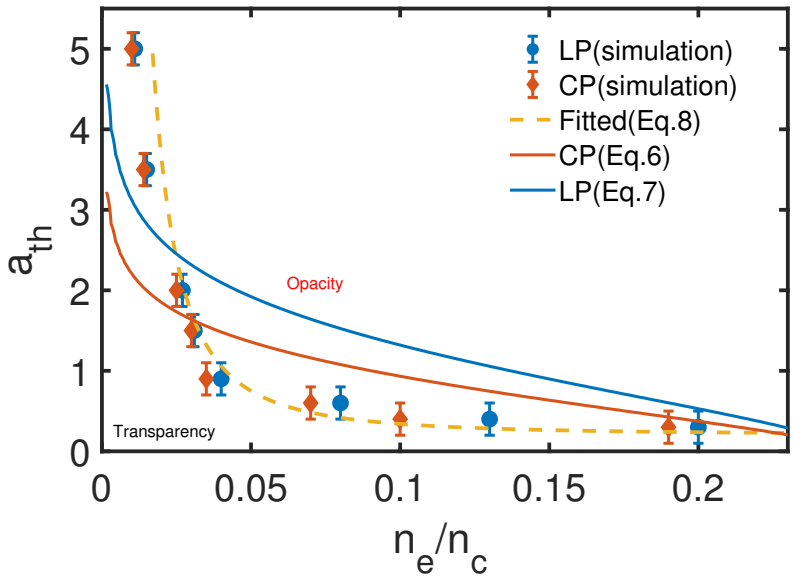

Figure 6. The threshold laser amplitude (a_{th}) for the relativistic-induced opacity as a function of the plasma density. The theoretical thresholds estimated by Eqs. (6) and (7) are compared with those obtained from the PIC simulations for both the circular polarization (CP) and linear polarization (LP) cases. The fitted thresholds by Eq. (8) are drawn for comparison. The initial underdense e^-e^+ plasma will become opaque under the irradiation of a relativistic laser pulse with $a \geq a_{th}$.

threshold laser amplitude a_{th}

$$4\left(a_{th}\sqrt{\frac{n_c}{2n_e}}+1\right)^3\frac{n_e}{n_c}=\left(2a_{th}\sqrt{\frac{n_c}{2n_e}}+1\right)^{3/2} \qquad \text{for CP,} \tag{6}$$

$$4\left(a_{th}\sqrt{\frac{n_c}{4n_e}}+1\right)^3\frac{n_e}{n_c}=\left(2a_{th}\sqrt{\frac{n_c}{4n_e}}+1\right)^{3/2} \qquad \text{for LP.} \tag{7}$$

The numerical solutions of Eqs. (6) and (7) are compared with the PIC simulation results in Fig.6. For a given e^-e^+ plasmas density, a series of PIC simulations with a varying laser amplitude are performed to draw the border between the transparency and relativistic-induced opacity regions. It is clear that the relativistic-induced opacity can be easily achieved by a weakly relativistic laser pulse ($0.1 \leq a \leq 1$) if the e^-e^+ plasma density is not to low ($n_e \geq 0.05n_c$). However, the threshold laser amplitude (a_{th}) for the relativistic-induced opacity increases dramatically with the decreasing e^-e^+ plasma density if $n_e \leq 0.05n_c$. This means that to accumulate enough electrons and positrons ahead of the laser pulse in a low-density e^-e^+ plasma an ultra-intense laser pulse must be applied.

The deviations between the theoretical estimations and the simulation results may be because the plasma density of the piled-up layer is assumed to uniform in the theoretical model. While the plasma density of the piled-up layer obtained from the simulation is not uniform as shown in Fig. 2. As an alternative, we find that the

relation

$$a_{th} \simeq 0.20287 + 0.00137 n_c^2/n_e^2 \tag{8}$$

fits the PIC simulation results quiet well, as shown in Fig. 6.

On the other hand, the relativistic-induced opacity can be regarded as the critical density decrease of e^-e^+ plasmas under the irradiation of relativistic laser pulses. With the increase of the laser intensity, the critical density of the e^-e^+ plasma decreases from the normal value $0.5n_c$ towards zero as shown in Fig.6. This is because that the electrons and positrons can more easily and quickly accumulate at the front of the laser pulse when they are pushed by the enhanced laser ponderomotive force with the increasing laser intensity. As a result, a denser e^-e^+ layer can be formed ahead of the laser pulse, which finally will prevent the penetration of the laser pulse into the e^-e^+ plasma. This is exactly opposite to the relativistic-induced transparency of electron-ion plasmas, in which the critical density of the electron-ion plasma increases with the increasing laser intensity.

Similar to the relativistic-induced transparency of electron-ion plasmas, the relativistic-induced opacity of e^-e^+ plasmas is essentially a one-dimensional effect and will take place in multi-dimensional cases as well. However, a higher laser amplitude (a_{th}) would be required to achieve this effect since the electrons and positrons will not be only longitudinally pushed but also transversely expelled by the laser radiation pressure in multi-dimensional cases. Further, the electromagnetic instabilities as well as the self-focusing and filamentation instabilities may disturb or even terminate the relativistic-induced opacity in the later stage of the relativistic laser interaction with the underdense e^-e^+ plasma.

3. Discussion

3.1. Reflectivity

The reflectivity, defined as the fraction of reflected radiant energy, is usually equal to the intensity ratio of the reflected light to the incident light if the reflector is at rest. In the relativistic-induced opacity scenario, however, the laser-plasma interface plays the role of a relativistically moving reflector. In this scenario, the reflectivity should be modified as the ratio of the reflected light intensity I'_{re} to the incident light intensity I'_{in} in the comoving frame with the laser-plasma interface. From the relativistic Doppler shift and the conservation of photon number, the relations $I'_{in} = I_{in}(1-\beta_b)/(1+\beta_b)$ and $I'_{re} = I_{re}(1+\beta_b)/(1-\beta_b)$ can be obtained, where I_{in} and I_{re} are respectively the incident and reflected light intensities in the laboratory frame of reference. Consequently, the reflectivity in the relativistic-induced opacity of e^-e^+ plasmas can be calculated as

$$R = \frac{I'_{re}}{I'_{in}} = \frac{I_{re}}{I_{in}} \left(\frac{1+\beta_b}{1-\beta_b}\right)^2 . \tag{9}$$

In Fig. 7(a), the reflectivity obtained from PIC simulations is displayed as a function of the laser amplitude a for a given e^-e^+ plasma density $n_e = 0.1n_c$. We find that the

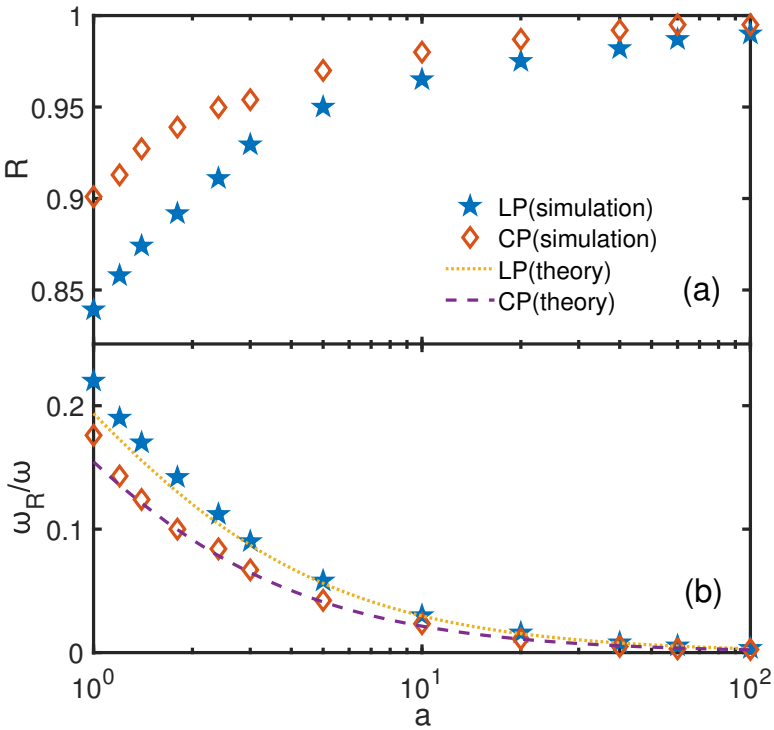

Figure 7. (a) The reflectivity R, and (b) the reflected light frequency ω_R as functions of the laser amplitude a in the relativistic-induced opacity of an underdense e^-e^+ plasma with $n_e = n_+ = 0.1n_c$. The theoretical reflected light frequency estimated by Eq. (10) are compared with the PIC simulation results for both the linear polarization (LP) and circular polarization (CP) cases.

reflectivity is quite high in the relativistic-induced opacity scenario of e^-e^+ plasmas. More importantly, the reflectivity increases with the increasing laser amplitude a. This indicates that the relativistic-induced opacity of an e^-e^+ plasma is more obvious at a higher laser intensity.

3.2. Potential Applications

Firstly, it is worth pointing out that the reflected light will be red shifted as follows

$$\omega_R = \omega \frac{1-\beta_b}{1+\beta_b} \tag{10}$$

due to the relativistic Doppler effect, where ω_R is the reflected light frequency. As illustrated in Fig. 7(b), the reflected light frequency ω_R estimated by using Eqs. (3) and (10) are in good agreement with those obtained from the PIC simulations in both circular and linear polarization cases. More importantly, the reflected light frequency ω_R is significantly red shifted to one fifth or even one tenth of the frequency of the incident light. With a larger laser amplitude a, the red shift of the reflected light is more obvious since the laser-plasma interface (as the reflector) moves faster in this case. This may provides an alternative approach to the generation of intense mid-infrared lights for broad applications. On the other hand, the red shift of the reflected light

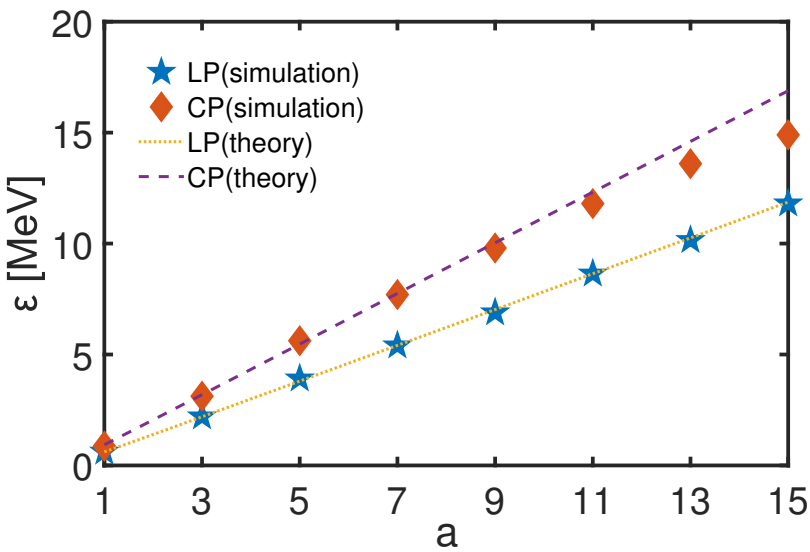

Figure 8. The mean energy of the accelerated positrons as a function of the laser amplitude in the relativistic-induced opacity of an e^-e^+ plasma with $n_e = n_+$=0.1 n_c. The theoretical energy estimated by Eq. (4) are drawn for comparison. The accelerated electrons have the same mean energy.

may also provide a useful approach to the diagnostics of the relativistic-induced opacity effect in the experiments.

Secondly, we notice that the e^-e^+ plasma as a whole can be accelerated to a relativistic speed in the relativistic-induced opacity scenario. We want to emphasize that the positrons and electrons are accelerated together and directly by the laser radiation pressure in this scenario, since they have the same masses. Further, there is nearly no charge separation in the e^-e^+ plasmas. More importantly, the positrons and electrons can be efficiently accelerated to high energies by such a direct radiation pressure acceleration (RPA) due to their small masses. This is different from the so-called RPA of ions in the interaction of intense laser pulses with electron-ion plasmas. In the RPA of ions, the laser radiation pressure first pushes the electrons forward and results in a charge separation between the electrons and the ions, and then the ions are actually accelerated by the charge separation field. The mean energy of the accelerated positrons and electrons is plotted in Fig.8 as a function of the laser amplitude for a given plasma density $n_e = n_+$=0.1 n_c. Moreover, the accelerated positron and electron beam may not suffer from the Coulomb expansion since the accelerated e^-e^+ plasma always remains quasi-neutral. Therefore, the direct radiation pressure acceleration in the relativistic-induced opacity of e^-e^+ plasmas may be a novel efficient mechanisms for the generation of energetic particles in the universe.

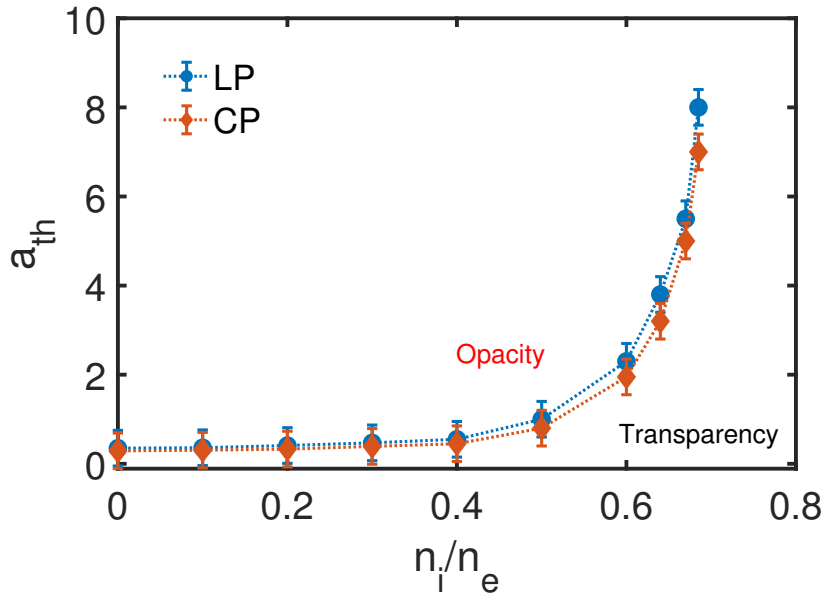

Figure 9. The threshold laser amplitude (a_{th}) for the relativistic-induced opacity of an underdense electron-positron-ion plasma as a function of the percentage of the ion charge number. The ions are assumed to be the protons with a mass $m_i = 1836m_e$, and an initial temperature of 100 eV. The plasma remains quasi-neutral with $n_i + n_+ = n_e = 0.1n_c$, where n_i is the ion number density.

3.3. Effect of Impurity Ions

Since a certain amount of ions will often coexist with the positrons and electrons, we also investigate the relativistic-induced opacity of underdense electron-positron-ion plasmas. If the percentage of the ion charge number is less than half, we find that the existence of the ions has a weak influence upon the threshold laser amplitude (a_{th}) for the relativistic-induced opacity as shown in Fig.9. However, a_{th} increases dramatically with the increasing ion charge number ratio if the latter is more than half. Specifically, a_{th} goes to infinity if $n_i/n_e \to 1$. This means that the relativistic-induced opacity cannot take place in an underdense conventional electron-ion plasma. In an overdense electron-ion plasma, however, the physics will be richer and more complicated. With the increase of the laser intensity, an initial overdense electron-ion plasma will first become relativistically transparent. With the further increase of the laser intensity, however, this relativistically transparent electron-ion plasma will become opaque again at extremely high laser intensities ($a \sim 1000$) [38].

4. Summary

In summary, we have found that an initial underdense e^-e^+ plasma can become opaque under the irradiation of a relativistically intense electromagnetic wave because of the efficient pile-up of the electrons and positrons at the front of the relativistic laser pulse. This relativistic-induced opacity of e^-e^+ plasmas is in marked contrast to the relativistic-

induced transparency of conventional electron-ion plasmas. The relativistic-induced opacity of e^-e^+ plasmas is essentially a one-dimensional effect, and it will take place in multi-dimensional cases as well. More importantly, this relativistic-induced opacity effect may provide an alternative way to the generation of intense mid-infrared lights and the production of energetic positrons. As a fundamental effect in e^-e^+ plasmas, this relativistic-induced opacity of underdense e^-e^+ plasmas could be of wide interest for both plasma physics and astrophysics. The construction of multi-PW lasers, such as the Extreme Light Infrastructure (ELI) [46] and Centre Interdisciplinaire Lumière EXtrême (CILEX) [47], may offer the opportunity to generate high density e^-e^+ plasmas for the experimental verification of this relativistic-induced opacity effect.

Acknowledgments

The work was supported by the National Natural Science Foundation of China (Grant Nos. 11675108, 11975154, 11721091, and 11775144), Science Challenge Project (No.TZ2018005) and EPSRC (Grant No. EP/R006202/1). The authors would like to acknowledge the OSIRIS Consortium, consisting of UCLA and IST (Lisbon, Portugal) for the use of OSIRIS. Simulations were performed on the Supercomputer at Shanghai Jiao Tong University.

References

[1] Ruffini R, Vereshchagin G and Xue S S 2010 Electron-positron pairs in physics and astrophysics: from heavy nuclei to black holes *Physics Reports* 487(1-4), 1-140

[2] Blandford R D and Znajek R L 1977 Electromagnetic extraction of energy from Kerr black holes *Monthly Notices of the Royal Astronomical Society* 179(3), 433-456

[3] Della T S, Gervasi M, Rancoita P G, Rozza D and Treves A 2015 Pulsar Wind Nebulae as a source of the observed electron and positron excess at high energy: The case of Vela-X *Journal of High Energy Astrophysics* 8, 27-34

[4] Romero G E, Boettcher M, Markoff S and Tavecchio F 2017 Relativistic jets in active galactic nuclei and microquasars *Space Science Reviews* 207(1-4),5-61

[5] Wardle J F C, Homan D C, Ojha R and Roberts D H 1998 Electron-positron jets associated with the quasar 3C279 *Nature* 395(6701), 457

[6] Abdo A A, Ackermann M *et al* 2009 Fermi observations of high-energy gamma-ray emission from GRB 080916C *Science* 323, 5922

[7] Lyne A G, Burgay M, Kramer M *et al* 2004 A double-pulsar system: a rare laboratory for relativistic gravity and plasma physics *Science* 303, 5661

[8] Strickland D and Mourou G 1985 Compression of amplified chirped optical pulses *Opt. Commun.* 56, 219-221 (1985)

[9] Remington B A, Drake R P and Ryutov D D 2006 Experimental astrophysics with high power lasers andZpinches *Reviews of Modern Physics* 78(3), 755-807

[10] Lebedev S V, Frank A and Ryutov D D 2019 Exploring astrophysics-relevant magnetohydrodynamics with pulsed-power laboratory facilities *Reviews of Modern Physics* 91(2)

[11] Chen H, Fiuza F *et al* 2015 Scaling the yield of laser-driven electron-positron jets to laboratory astrophysical applications *Physical review letters* 114(21), 215001

[12] Del Sorbo D, Blackman D R *et al* 2018 Efficient ion acceleration and dense electron-positron

plasma creation in ultra-high intensity laser-solid interactions *New Journal of Physics* 20(3), 033014

[13] Schwinger J 1951 On gauge invariance and vacuum polarization *Physical Review* 82(5), 664

[14] Bethe H and Heitler W 1934 On the stopping of fast particles and on the creation of positive electrons *Proceedings of the Royal Society of London. Series A, Containing Papers of a Mathematical and Physical Character* 146(856), 83-112

[15] Nakashima K I and Takabe H 2002 Numerical study of pair creation by ultraintense lasers *Physics of Plasmas* 9(5), 1505-1512

[16] Chen H, Wilks S C *et al* 2009 Relativistic positron creation using ultraintense short pulse lasers *Physical review letters* 102(10), 105001

[17] Liang E, Clarke T *et al* 2015 High e^+/e^- ratio dense pair creation with $10^{21}Wcm^{-2}$ laser irradiating solid targets *Scientific reports* 5, 13968

[18] Sarri G, Poder K *et al* 2015 Generation of neutral and high-density electron-positron pair plasmas in the laboratory *Nature communications* 6, 6747

[19] Breit G and Wheeler J A 1934 Collision of two light quanta *Physical Review* 46(12), 1087

[20] Bell A R and Kirk J G 2008 Possibility of prolific pair production with high-power lasers *Physical review letters* 101(20), 200403

[21] Zhu X L, Yu T P, Sheng Z M, Yin Y, Turcu I C E and Pukhov A 2016 Dense GeV electron-positron pairs generated by lasers in near-critical-density plasmas *Nature communications* 7, 13686

[22] Liu J J, Yu T P, Yin Y, Zhu X L and Shao F Q 2016 All-optical bright γ-ray and dense positron source by laser driven plasmas-filled cone *Optics express* 24(14), 15978-15986

[23] Chang H X, Qiao B *et al* 2015 Generation of overdense and high-energy electron-positron-pair plasmas by irradiation of a thin foil with two ultraintense lasers *Physical Review E* 92(5), 053107

[24] Ridgers C P, Brady C S, Duclous R, Kirk J G, Bennett K, Arber T D and Bell A R 2012 Dense Electron-Positron Plasmas and Ultraintense γ rays from Laser-Irradiated Solids *Physical Review Letters* 108(16)

[25] Lécz Z, Andreev A 2019 Minimum requirements for electron-positron pair creation in the interaction of ultra-short laser pulses with thin foils *Plasma Physics and Controlled Fusion* 61(4), 045005

[26] Liu J X, Ma Y Y *et al* 2016 Enhanced electron-positron pair production by ultra intense laser irradiating a compound target *Plasma Physics and Controlled Fusion* 58(12), 125007

[27] Lobet M, Davoine X, d'Humières E and Gremillet L 2017 Generation of high-energy electron-positron pairs in the collision of a laser-accelerated electron beam with a multipetawatt laser *Physical Review Accelerators and Beams* 20(4), 043401

[28] Stewart G and Laing E 1992 Wave propagation in equal-mass plasmas *Journal of Plasma Physics* 47(2), 295-319

[29] Zank G P, Greaves R G 1995 Linear and nonlinear modes in nonrelativistic electron-positron plasmas *Physical Review E* 51(6), 6079

[30] Iwamoto N 1993 Collective modes in nonrelativistic electron-positron plasmas *Physical Review E* 47(1), 604

[31] Edwards M R, Fisch N J and Mikhailova J M 2016 Strongly enhanced stimulated Brillouin backscattering in an electron-positron plasma *Physical review letters* 116(1), 015004

[32] Marburger J H and Tooper R F 1975 Nonlinear optical standing waves in overdense plasmas *Physical Review Letters* 35(15), 1001

[33] Lefebvre E and Bonnaud G 1995 Transparency/opacity of a solid target illuminated by an ultrahigh-intensity laser pulse *Physical review letters* 74(11), 2002

[34] Goloviznin V V and Schep T J 2000 Self-induced transparency and self-induced opacity in laser-plasma interactions *Physics of Plasmas* 7(5), 1564-1571

[35] Palaniyappan S, Hegelich B M *et al* 2012 Dynamics of relativistic transparency and optical shuttering in expanding overdense plasmas *Nature Physics* 8(10), 763

[36] Weng S M, Mulser P and Sheng Z M 2012 Relativistic critical density increase and relaxation and

high-power pulse propagation *Physics of Plasmas* 19(2), 022705

[37] Weng S M, Murakami M, Mulser P and Sheng Z M 2012 Ultra-intense laser pulse propagation in plasmas: from classic hole-boring to incomplete hole-boring with relativistic transparency *New Journal of Physics* 14(6), 063026.

[38] Ji L L, Shen B F and Zhang X M 2018 Transparency of near-critical density plasmas under extreme laser intensities *New Journal of Physics* 20(5), 053043

[39] Cattani F, Kim A, Anderson D and Lisak M 2000 Threshold of induced transparency in the relativistic interaction of an electromagnetic wave with overdense plasmas *Physical Review E* 62(1), 1234

[40] Robinson A P L, Trines R M G M, Dover N P and Najmudin Z 2012 Hole-boring radiation pressure acceleration as a basis for producing high-energy proton bunches *Plasma Physics and Controlled Fusion* 54(11), 115001

[41] Fonseca R A, Silva L O *et al* 2002 OSIRIS: A three-dimensional, fully relativistic particle in cell code for modeling plasma based accelerators. In International Conference on Computational Science (pp. 342-351). Springer, Berlin, Heidelberg

[42] Crannell C J, Joyce G, Ramaty R and Werntz C 1976 Formation of the 0.511 MeV line in solar flares *The Astrophysical Journal* 210, 582-592

[43] Gould R J 1989 Direct positron annihilation and positronium formation in thermal plasmas *The Astrophysical Journal* 344, 232-238

[44] Robinson A P L, Gibbon P, Zepf M, Kar S, Evans R G and Bellei C 2009 Relativistically correct hole-boring and ion acceleration by circularly polarized laser pulses *Plasma Physics and Controlled Fusion* 51(2), 024004

[45] Schlegel T, Naumova N, Tikhonchuk V T, Labaune C, Sokolov T V and Mourou G 2009 Relativistic laser piston model: Ponderomotive ion acceleration in dense plasmas using ultraintense laser pulses *Physics of Plasmas* 16(8), 083103

[46] ELI Extreme Light Infrastructure. http://www.eli-beams.eu

[47] Centre Interdisciplinaire Lumière EXtrême (CILEX) https://portail.polytechnique.edu/luli/en/cilex-apollon/cilex